Full Determination of the Rotational Diffusion Tensor by Electron Paramagnetic Resonance at 250 GHz†

David E. Budil,‡ Keith A. Earle, and Jack H. Freed*

Baker Laboratory of Chemistry, Cornell University, Ithaca, New York 14853

Received: July 30, 1992; In Final Form: October 8, 1992

High-frequency (250 GHz) electron paramagnetic resonance (EPR) spectra in the limit of motional narrowing have been studied for a nitroxide spin probe diffusing in a low-viscosity isotropic solvent. The enhanced sensitivity of the 250-GHz spectrum to rotational modulation of the g tensor reveals new details of the microscopic motion of the spin probe. Specifically, it is shown how independent linear constraints imposed by line-width measurements at 250 GHz and a lower frequency may be used to fully determine the diffusion tensor $\mathbf{R}$ in the general case $R_x \neq R_y \neq R_z$. This procedure is demonstrated experimentally for the perdeuterated Tempone (PDT) probe diffusing in toluene-d_8, where analysis of the line widths obtained at 250 and 9.5 GHz gives values for the anisotropy parameters $\rho_x = R_x/R_z$ and $\rho_y = R_y/R_z$ of 1.8 ± 0.2 and 1.5 ± 0.3, respectively. Thus, this molecule is found to exhibit small deviations from spherically symmetric reorientation. The enhanced accuracy of determining the g tensor from rigid-limit spectra obtained at 250 GHz is an important feature of such high-frequency studies. Existing theoretical expressions for motionally narrowed nitroxide line widths have been modified appropriately for the high-field case by including a completely anisotropic diffusion tensor and the ^{14}N nuclear Zeeman interaction, which becomes important at fields above about 5 T.

Introduction

The utility of EPR spin relaxation studies for probing microscopic molecular motions has been demonstrated in a broad variety of systems, including isotropic solvents,[1-3] liquid crystals,[4,5] model membranes,[6] and spin-labeled biomolecules. Many dynamic processes of interest fall into the motional narrowing limit for EPR spectroscopy, in which the product of the correlation time τ_R characterizing the motion and the magnitude of the orientation-dependent part of the spin Hamiltonian (in frequency units) is much less than unity.

However, spin relaxation in the fast-motional regime does not in general reflect many of the details of the rotational dynamics. For example, although the fast-motional line widths are sensitive to the rotational anisotropy of a spin probe, it is usually not possible to determine the rotational diffusion tensor $\mathbf{R}$ fully, and additional assumptions about the motion are usually introduced. In some cases, additional details of the microscopic dynamics can influence the linewidths, and it would be desirable to have a means of discriminating between such influences and the effects of rotational anisotropy.

Previous fast-motional studies of small spin probes such as perdeuterated 2,2',6,6'-tetramethyl-4-piperidone-1-nitroxide (pd-Tempone, or PDT) have shown that their rotational dynamics may indeed deviate appreciably from simple diffusive behavior in a wide variety of solvents.[2-4,7] Several distinct models have emerged to account for the influence of microscopic interactions on the spin probe diffusion. In isotropic solvents, studies of nitroxide linewidths have led to a model that explicitly includes fluctuating local torques exerted by the solvent molecule on the probe, which have relaxation times comparable to τ_R.[2] In contrast, the anomalous line-width behavior observed for PDT in many liquid-crystal solvents suggests that in these solvents the intermolecular torques may persist on a time scale longer than τ_R,[4] corresponding to a transient local solvent structure around the spin probe. In studies of PDT in toluene-d_8 in which τ_R was varied as a function of pressure[3] as well as temperature, no evidence of effects of a transient local solvent structure was found, as one might expect; instead, substantial evidence for a fluctuating torques model was found.

In the past[1-4] one has been partially successful in distinguishing between these various aspects of the molecular dynamics by studying the motionally narrowed spectra over a substantial temperature (and/or pressure) range. Then by utilizing the data only over that range for which $\omega_e^2\tau_R^2 \gg 1$ (where ω_e is the EPR resonance frequency) it is possible to obtain information about the anisotropy of $\mathbf{R}$, provided an assumption of axial symmetry is made, and for which a Brownian reorientational model is utilized. This is because the data supply one key constraint, which is usually temperature-independent. (It is also necessary to specify the orientations of the magnetic tensors with respect to the principal axis of $\mathbf{R}$.) Following this, the data for $\omega_e^2\tau_R^2 \leq 1$ (i.e., in the limit of extreme motional narrowing) are analyzed with the already estimated $\mathbf{R}$. Any deviations between the prediction and experiment in this motional regime are then interpreted in terms of a simple model of fluctuating local torques.

One strategy to better discriminate these matters is to study the fast-motional line-width behavior of the spin label as a function of EPR frequency. In the present work, we have extended our extensive previous electron spin relaxation studies[2,3] of the PDT probe in the simple solvent toluene-d_8 to a very high EPR frequency (250 GHz). At this frequency, virtually all the data satisfy the condition $\omega_e^2\tau_R^2 \gg 1$, so it is available for study of the rotational diffusion tensor, $\mathbf{R}$. We do indeed find that the high-field fast-motional spectra are particularly sensitive to the details of $\mathbf{R}$. In theory, we find that such high-frequency measurements are sufficient to determine all the components of $\mathbf{R}$ in the context of a Brownian rotation model (again provided the orientations of the magnetic tensors relative to the principal axes of $\mathbf{R}$ are specified). This follows because two key constraints (usually temperature independent) are in principle now available. In practice, we are able to achieve this goal by combining the fast-motional measurements at 250 GHz with those obtained at a lower frequency (e.g., 9.5 GHz) in order to eliminate the need to resolve line-width components that contribute relatively very weakly to the 250-GHz spectra, but contribute substantially at 9.5 GHz. (The principal axes of magnetic and diffusion tensors are all taken to be colinear in keeping with details of molecular

† Supported by NIH Grant GM 25862 and NSF Grant CHE9004552.
‡ NIH NRSA GM-12924 recipient.

0022-3654/93/2097-1294$04.00/0

shape and structure that have been discussed in detail previously[2-4]).

Our purpose in the present work is to demonstrate the utility of high-frequency EPR in the fast-motional regime. The considerable value of slow-motional EPR studies for motional dynamics has been demonstrated in the past at lower frequencies.[1-4] Such studies can provide results which enable one to distinguish such non-Brownian features as reorientation by strong vs weak jumps, a matter not readily accessible to studies based on fast-motional spectra. However, the analyses of the slow-motional spectra that are required are rather complex compared to the simpler analyses of motionally narrowed spectra. Preliminary results obtained in this laboratory do indicate the enhanced sensitivity of the slow-motional spectra at 250 GHz to such questions of non-Brownian behavior, a matter we plan to discuss in a future report.

The analysis of fast-motional spectra at 250 GHz may typically be simplified compared to conventional EPR frequencies because the rotationally induced homogeneous line widths are usually much larger than the inhomogeneous widths at this frequency, in which case the spectral lines are well-approximated by Lorentzian line shapes. Moreover, line-broadening effects due to spin-rotational coupling and Heisenberg exchange are comparatively small, so that the line widths more clearly reflect the reorientational dynamics of the probe.

Experimental Methods and Results

EPR Spectroscopy. Most of the features of the 250-GHz EPR spectrometer used in this work have been described previously.[8,9] Briefly, the sample is placed in a semiconfocal Fabry–Perot transmission cavity at the point of maximum field homogeneity in a sweepable superconducting magnet. The 250-GHz radiation is generated by a solid-state source located below the magnet, propagated as a Gaussian beam along the magnet bore via a series of Teflon lenses, and introduced into the cavity via a conical feedhorn antenna and coupling hole. After passing through the cavity, the signal is reconverted to a Gaussian mode and propagated to a waveguide-mounted diode detector. The EPR signal is obtained using the standard method of field modulation and phase-sensitive detection. To optimize spectrometer sensitivity for the small sample volumes used in this work, the dc power supply used to bias the detector was replaced with rechargable NiCd batteries.

The open resonator design of our spectrometer requires a much different sample geometry than that used in standard microwave cavities. Since the wavelength of the 250-GHz radiation (1.2 mm) is somewhat smaller than the sample dimensions, scattering and diffraction losses can seriously degrade the quality factor of the resonator. Previous EPR work at 250 GHz has been carried out with reusable Teflon holders with flat windows for solids, liquids, and liquid crystals in the temperature range −100 to 100 °C.[8,9] While this type of holder minimizes interference with the millimeter-wave beam in the resonator, it is not sealable and requires that the magnet bore be continuously purged with dry nitrogen gas in order to reduce line broadening from molecular oxygen. Although the oxygen that remains dissolved in the Teflon can be removed by extensive pumping or purging with purified nitrogen gas at elevated temperatures, such measures have proved unnecessary for most applications, since any residual broadening is generally much smaller than the EPR linewidths of interest at 250 GHz.

However, for fast-motional studies at 250 GHz, we found that more rigorous methods were needed to exclude oxygen from the sample. In low-viscosity solvents at room temperature and above, the relatively rapid rotational diffusion of the small PDT probe produces rather narrow EPR lines even at 250 GHz, and the spectra are quite sensitive to small amounts of molecular oxygen. For this type of sample, we have been able to use short sealed quartz tubes that have been deoxygenated by standard freeze–pump–thaw methods by placing the tube axis transverse to the beam direction in the cavity.

To prepare a deoxygenated sample for use in our 250-GHz spectrometer, a quartz tube with a wall thickness of approximately 1 mm and an o.d. of 4–5 mm is sealed at its end, filled to a height of 10–20 mm, and degassed on a vacuum line. While under vacuum, the sample is held under liquid nitrogen with cork-covered forceps and sealed with a microtorch as close as possible to the liquid surface. The curvature and wall thickness of the sample tubes produce appreciable scattering losses in the cavity (as monitored by its transmission of the 250-GHz radiation), which were minimized by carefully centering the tube on the coupling hole of the cavity and adjusting the height of the tube above the flat mirror surface using a tube support machined from Teflon. The tube was canted at an angle of approximately 5° from the horizontal to avoid interference from the small bubble that inevitably remained after the sealing procedure.

The sample tubes also affected minimum observable EPR line width, which varied from 0.75 to 1.25 G in motionally narrowed spectra (cf. below) depending on the diameter of the tube and the orientation of the tube axis with respect to the known plane of E-field polarization of the incident 250-GHz radiation. This minimum width is larger than the axial magnetic field inhomogeneity of 0.27 G specified by the manufacturer of the magnet, which was verified using a ^{2}H NMR gaussmeter (Sentec Model 1101). These observations suggest that the combined small radius and large refractive index of the quartz sample tube may distort the incident beam sufficiently to illuminate regions sample outside the 10-mm sphere spherical volume of highest field homogeneity, thereby leading to more substantial line broadening by field inhomogeneity. The degree of the distortion would then depend on the angle between the axis of curvature and the E field of the millimeter waves, consistent with our observations. For the present work, the tube diameter and orientation were chosen to obtain the smallest residual broadening available.

Toluene-d_8 (99.95% D) was obtained from Aldrich and used without further purification other than drying over molecular sieves. The PDT was obtained from a stock prepared locally by synthetic procedures described previously[2] and purified by vacuum sublimation. A 4.0 mM stock solution was prepared by dissolving a weighed amount of crystalline PDT with overnight stirring at room temperature; sample aliquots were diluted to 0.5 mM in order to minimize line width due to Heisenberg exchange. The sample temperature was controlled to within 1 °C by a combination of dry nitrogen flow and heater resistors mounted on the lower mirror of the cavity and monitored by copper–constantan thermocouples placed next to the sample tube and fixed in the lower cavity mirror.

Measurement of Magnetic Tensors. An established advantage of very high frequency EPR is the much greater resolution for measurement of the g tensor, as well as improved resolution for the hyperfine tensor.[9,10] The magnetic tensors of PDT in toluene-d_8 were determined from a near-rigid limit spectrum of this system obtained at 250 GHz below −130 °C, shown in Figure 1. The field sweep was calibrated using a Mn^{2+}/MgO EPR standard and also using the ^{2}H NMR gaussmeter. The magnetic parameters measured at 250 GHz are given in Table I, together with the values used in previous 9.5-GHz work,[2] and also those reported for Tempone in toluene at 148 GHz[10] for comparison. One should note the much greater accuracy for the measurement of g-tensor components at the higher frequencies, especially for the differences between the g-tensor principal values (e.g., $g_x - g_y$), which depend on the relative errors (cf. Table I), and are the important quantities for spin relaxation studies. (It should also be noted that whereas there are significant differences between the g-tensor values we obtained at 250 GHz and those reported for 148 GHz, the *differences* in principal values are of the order of the relative errors in the 148-GHz data. The discrepancy in absolute values is most likely due to differences in absolute field calibration.) The 250-GHz results were used in the present study.

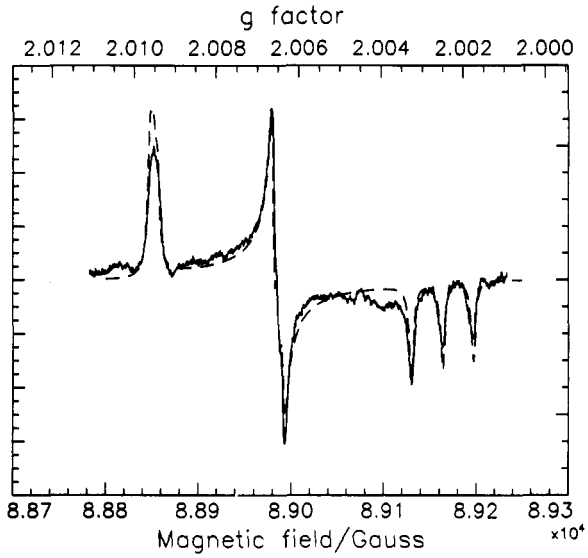

Figure 1. The 250-GHz EPR spectrum of 0.5 mM pd-Tempone in toluene-d_8 obtained below −130 °C. The sample was contained in a sealed quartz tube as described in the text. The dotted line shows the spectral simulation using the magnetic parameters given in Table I; inhomogeneous broadening was included in the simulation by convolution of the spectrum with a Lorentzian line with 2.7 G-peak-to-peak width.

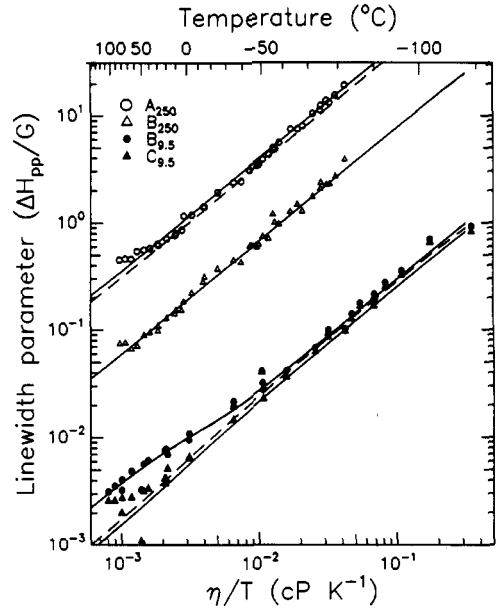

Figure 2. Dependence of A and B measured at 250 GHz and B and C measured at 9.5 GHz (data from ref 2) for pd-Tempone in toluene-d_8 as a function of η/T. Solid lines: calculated η/T dependence of linewidth parameters for the model of anisotropic Brownian motion with the 250-GHz magnetic parameters given in Table I, assuming rotational anisotropy of $\rho_x = 1.8$ and $\rho_y = 1.5$. Dashed lines: best fit assuming isotropic diffusion. Note $\epsilon = 4.5$ (cf. text).

The (inhomogeneous) line broadening of the rigid limit spectrum referred to in Figure 1 is somewhat larger than at 9.5 GHz (2.7 vs 1.2 G for an assumed Lorentzian distribution). Aside from any extra magnetic field inhomogeneities at the higher frequency (cf. above) this difference is very likely due to a small amount of g strain, i.e., local site variations in the g values, which are amplified by the ratio of the magnetic fields, or a factor of 26 in the 250-GHz spectra compared to 9.5 GHz. A small g-strain contribution of ca. 1 G at 250 GHz would be insignificant at 9.5 GHz.

Line-Width Measurements. At 250 GHz, most of the experimental motionally narrowed lines were broad enough (1 G or more) that the inhomogeneous line width due to superhyperfine coupling with the 12 equivalent methyl deuterons of PDT could be neglected, based on the earlier analysis of Polnaszek and Freed,[4] which we have confirmed. This feature facilitated the analysis of the 250-GHz data, which was accomplished by fitting a simple sum of three Lorentzian lines to the experimental spectrum. In contrast, line widths measured at 9.5 GHz must be corrected for these inhomogeneous effects using a convolution of the underlying Lorentzian line shape with a Gaussian envelope corresponding to 12 equivalent spin-1 nuclei. Our fitting method was the modified Levenberg–Marquardt nonlinear least-squares algorithm from the MINPACK subroutine library.[11]

Fast-Motional Analysis. In the fast-motional limit, the dependence of the line width T_2^{-1} upon the nuclear quantum number m_I associated with a given spectral line may be expressed in terms of the line-width parameters A, B, and C:

$$T_2^{-1}(m_I) = A + Bm_I + Cm_I^2 \qquad (1)$$

The linewidth parameters were determined from experimental 250-GHz spectra taken over the temperature range −85 to 90 °C for 0.5 mM PDT in toluene-d_8.

At 250 GHz, the A and B terms are found to be much larger than the C term for reasons discussed below. As a result, the C parameter proved difficult to determine accurately at 250 GHz because of its very small magnitude in comparison to the overall linewidths, which are dominated by A and B. That is, large uncertainties arise in the value of C because it is calculated by taking the difference of large quantities. We therefore excluded the C parameter measured at 250 GHz from our analysis. Our measured values of A and B at 250 GHz (hereafter referred to as A_{250} and B_{250}) are shown in Figure 2.

On the other hand, at 9.5 GHz, just the B and C terms (hereafter $B_{9.5}$ and $C_{9.5}$) are utilized[1-4] (cf. below). Preliminary experiments on aliquots of the solutions used for 250 GHz were performed at 9.5 GHz. They were found to give results consistent with the previous data of Hwang et al.[2] The extensive dataset of Hwang et al. on B and C (shown in Figure 2) was utilized in our analysis.

TABLE I: Magnetic Parameters Measured from Rigid-Limit Samples at 250 and 9.5 GHz for Perdeuterated Tempone in Toluene-d_8 and at 148 GHz for Tempone in Toluene

	250 GHz[a,b]	148 GHz[c,d]	9.5 GHz[b,e]
g_x	2.00936 ± 3 × 10⁻⁵ [k]	2.00918 ± 7 × 10⁻⁵ [l]	2.0096 ± 2 × 10⁻⁴
g_y	2.00633 ± 3 × 10⁻⁵ [k]	2.00620 ± 7 × 10⁻⁵ [l]	2.0063 ± 2 × 10⁻⁴
g_z	2.00233 ± 3 × 10⁻⁵ [k]	2.00220 ± 7 × 10⁻⁵ [l]	2.0022 ● 2 × 10⁻⁴
$\langle g \rangle$[f]	2.00601 ± 5 × 10⁻⁵	2.00586 ± 12 × 10⁻⁵	2.0060 ± 3 × 10⁻⁴
g_s[g]	2.00602[h]	2.00610 ± 4 × 10⁻⁵ [i]	2.00602 ± 5 × 10⁻⁵
A_x/γ_e	4.1 ± 0.2	4.8 ± 0.1	4.1 ± 0.5
A_y/γ_e	5.1 ± 0.2	5.4 ± 0.1	6.1 ± 0.5
A_z/γ_e	33.6 ± 0.2	33.3 ± 0.3	33.4 ± 0.2
$\langle A \rangle/\gamma_e$[j]	14.3 ± 0.3	14.5 ± 0.3	14.5 ± 0.7
a_N[g]	14.3 ± 0.2	14.3 ± 0.2	14.57 ± 0.02

[a] This work. [b] Parameters determined by spectral simulation. [c] From ref 10. [d] Parameters determined from spectrum without simulation. [e] From ref 2. [f] $\langle g \rangle = (g_x + g_y + g_z)/3$. [g] Measured in motionally narrowed region. [h] Calibrated to g_s measured for 0.1 mM PDT in toluene-d_8 at X-band, from ref 2. [i] Calibrated to g_s measured for peroxylamine disulfonate at X-band. [j] $\langle A \rangle = (A_x + A_y + A_z)/3$. [k] This absolute error is dominated by the calibration error; the relative error (i.e., the error in g_i relative to a calibration point in the spectrum) is estimated to be 5 × 10⁻⁶ from the spectral fits. [l] Absolute error quoted in ref 10. Relative error is estimated to be (3–5) × 10⁻⁵.

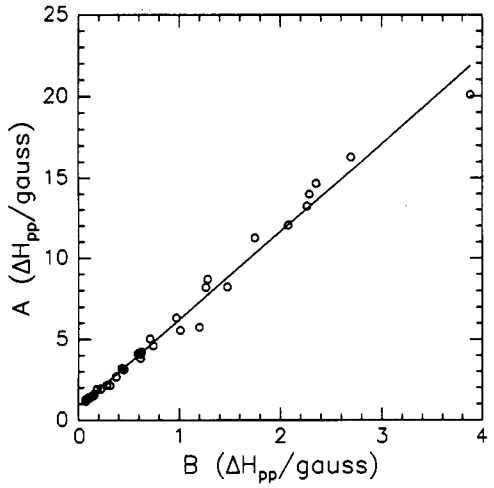

Figure 3. A_{250} and B_{250} line-width parameters measured for 0.5 mM pd-Tempone in toluene-d_8 over the temperature range −85 to 90 °C. Solid line: least-squares fit to the experimental points with a slope corresponding to A_{250}/B_{250} = 5.5 ± 0.1 and an intercept of 0.75 G.

However, our present 9.5-GHz experiments were utilized to determine the Heisenberg exchange rate as a function of concentration and temperature by standard methods.[12]

Confirmation of the self-consistency of the results at 250 GHz and at 9.5 GHz was provided by a comparison of B_{250} and $B_{9.5}$. We find from all our data (excluding the 9.5-GHz data for which $\eta/T < 10^{-2}$ cP/K, i.e., for which nonsecular terms begin to contribute) that the ratio of $B_{250}/B_{9.5}$ (26.2 ± 1.3) is exactly the ratio of the magnetic fields (=26.3) as required by the line-width theory (cf. below). The $C_{9.5}/B_{9.5}$ ratio is well-known to be constant over the range where $\eta/T > 10^{-2}$ cP/K[2,3] and is equal to 0.925 ± 0.016 for PDT in toluene-d_8.[2] It is this temperature-independent $C_{9.5}/B_{9.5}$ ratio which provides the key constraint usually utilized to obtain some information on rotational diffusional asymmetry from low frequency experiments.

To obtain the A_{250}/B_{250} ratio, which is the new key constraint needed to determine the anisotropy of rotational diffusion (cf. Discussion), we plotted A_{250} vs B_{250} over the range of temperatures studied, as shown in Figure 3. The data obey a linear relationship over this temperature range, and A_{250}/B_{250} could be obtained by a linear least-squares fit to the experimental data. This procedure gave A_{250}/B_{250} = 5.5 ± 0.1 and an intercept corresponding to a residual line width of 0.75 ± 0.20 G. This residual line width is larger than the expected frequency-independent contributions to A' (cf. eq 2) such as spin-rotation coupling and Heisenberg exchange and is typically a factor of 5 or more times larger than $A_{9.5}$ measured using aliquots of the same sample at temperatures below about 20 °C (cf. below). We have discussed above our observations which suggest that at least some of this residual width arises from inhomogeneity in the applied magnetic field.

We have carefully considered the sensitivity of the temperature-dependent part of the A_{250}/B_{250} ratio to the method of accounting for residual broadening of A_{250}. For example, we found that by varying the intercept by ±30%, the slope varied by only about ±0.1. We also refitted the A_{250} data to the functional form $a\eta/T + bT/\eta + c$, where $a\eta/T$ is the relevant contribution to A_{250} (i.e., A_{250}^{rel}), bT/η includes the sum of spin-rotational[2] (SR) and Heisenberg exchange (HE) contributions, and c is the presumed temperature-independent residual width. Again, we obtained A_{250}^{rel}/B_{250} = 5.5 ± 0.1 (and an estimate of b consistent with our 9.5-GHz measurements of SR and HE). That the A_{250}/B_{250} ratio is remarkably insensitive to the method of determining the residual width in A_{250} is due to the fact that over most of the temperature range studied (i.e. for $T < 20$ °C) A_{250}^{rel} is much greater than the other contributions.

The 250- and 9.5-GHz line-width parameters shown in Figure 2 are plotted as a function of η/T, which was calculated for toluene-d_8 using the experimentally measured temperature and the expression for $\eta(T)$ given by Barlow et al.,[13] corrected for the molecular weight difference due to perdeuteration of the solvent. The solid lines appearing in Figure 2 give the best fit to the experimental data utilizing an approach that will be discussed in detail in the next section.

We extensively investigated the η/T dependence of A_{250} and B_{250} using previous theoretical expressions for the fast-motional line widths of nitroxides,[2] modified to include the ^{14}N nuclear Zeeman energy as described in the Appendix. Several different models were used in our attempts to analyze the line-width data: (i) Brownian rotational diffusion, including the possibility of anisotropic rotation with an axial diffusion tensor;[2] (ii) fluctuating torques exerted by the solvent;[2,3] (iii) slowly relaxing local solvent structures.[3,4] It proved possible to fit the temperature dependence of both A_{250} and B_{250} using these models and including the refined measurement of the magnetic tensor parameters obtained at 250 GHz (cf. Table I). In general, since both A_{250} and B_{250} appear quite linear on a log–log plot vs η/T (after A_{250} is corrected for the residual line width) the data could be fit assuming simple Brownian motion without resorting to the more complex models, (ii) and (iii) noted above. In fact, as expected from the theory, the high-field line-width parameters proved particularly insensitive to the ϵ correction term that appears in the nonsecular spectral densities in the fluctuating torques model (cf. eq 3, next section), from which we conclude that the high-field data cannot in general be used to assess the presence of fluctuating torques in the motional dynamics.

However, using the available models we could not find a solution that *simultaneously* fit the line-width data obtained at 250 GHz and those measured for the same solvents at 9.5 GHz using any combination of parameters for any of the models investigated. This is most apparent when considering the A_{250}/B_{250} and $C_{9.5}/B_{9.5}$ ratios. Predictions for the A_{250} and B_{250} curves based on fits to the lower frequency results inevitably underestimated the A_{250}/B_{250} ratio. Given that $B_{250}/B_{9.5}$ equals the ratio of the two frequencies, this amounts to an underestimate of A_{250} based on the 9.5-GHz data. Conversely, solutions that fit the high-frequency data tended to overestimate $C_{9.5}/B_{9.5}$ over a key portion of the temperature range studied (i.e., $C_{9.5}$ was overestimated for $\eta/T > 10^{-2}$ cP/K), contrary to experimental observations. This consistent discrepancy suggested the possibility that an inadequate model was being used in the initial data analysis. Specifically, we found that relaxing the restriction of the diffusion tensor to axial symmetry provided the additional degree of freedom needed to obtain satisfactory fits to the linewidth data at both 250 and at 9.5 GHz, as we discuss in greater detail in the next section.

Discussion

General Considerations of Motional Narrowing at High EPR Frequencies. The effect of high magnetic fields on the fast-motional EPR spectrum of a nitroxide may be understood by considering the individual measurable spectral densities that contribute to each of the linewidth parameters A, B, and C:[1,2,4]

$$A - A' = 2J_1^{DD}(\omega_a) + {}^2/_3J_0^{DD}(\omega_e) + 4J_2^{DD}(\omega_e) + {}^8/_3J_0^{GG}(0) + 2J_1^{GG}(\omega_e)$$

$$B = {}^{16}/_3J_0^{DG}(0) + 4J_1^{DG}(\omega_e)$$

$$C = {}^8/_3J_0^{DD}(0) - J_1^{DD}(\omega_a) = {}^1/_3J_0^{DD}(\omega_e) + 2J_1^{DD}(\omega_e) - 2J_2^{DD}(\omega_e) \quad (2)$$

The J functions, or spectral densities, in this equation arise from rotational modulation of the electron-nuclear dipolar (END) tensor (J^{DD}), the electronic "g-tensor" (J^{GG}), and the correlated effect of both tensors (J^{DG}). The spectral densities needed are at frequencies $\omega = 0$, ω_a, and ω_e, where ω_e is the EPR resonance frequency and ω_a refers to the NMR frequency, as defined more

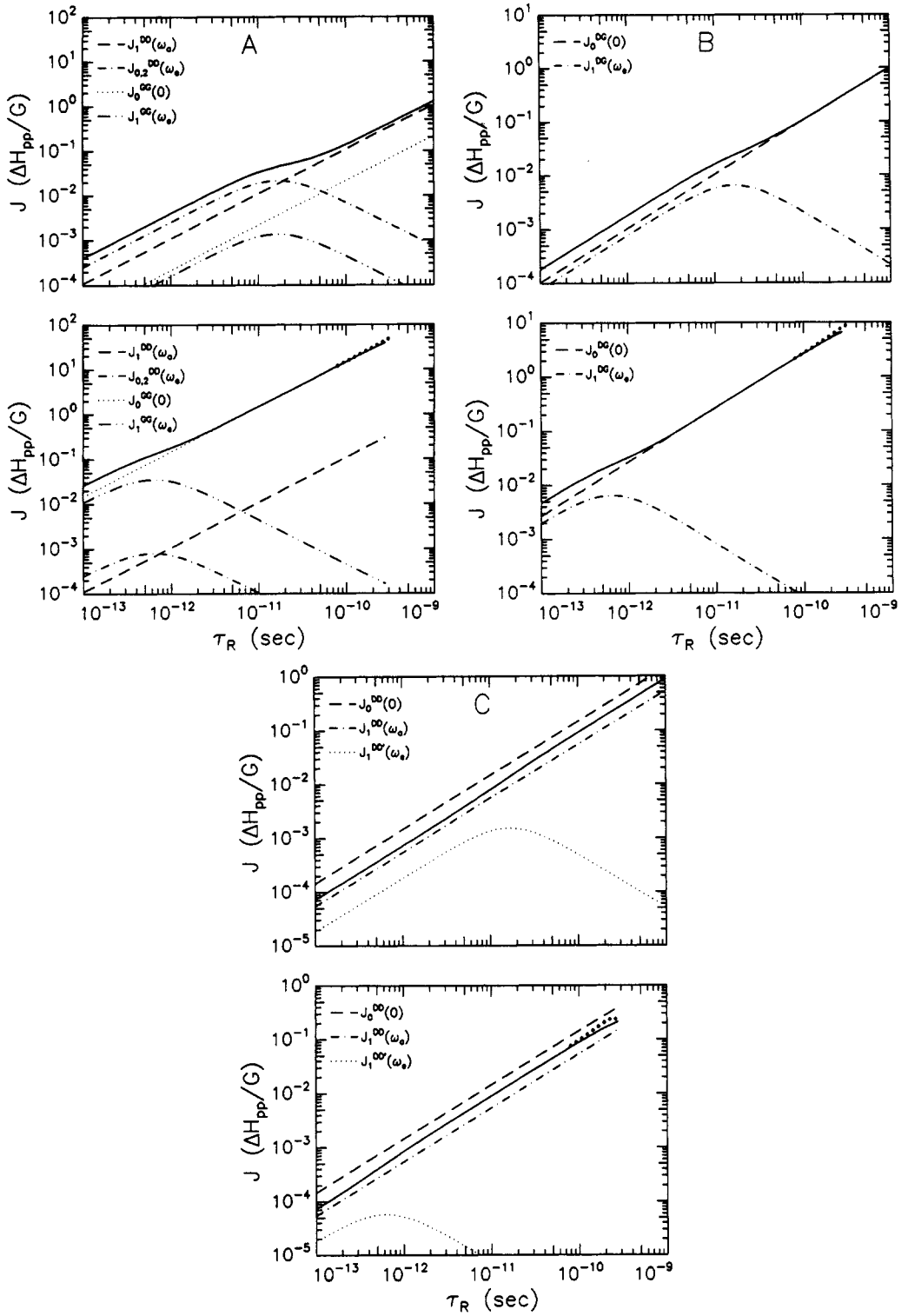

Figure 4. Theoretical calculation of measurable spectral densities as a function of τ_R at 250 and 9.5 GHz. (A)–(C) terms belonging to A–C, respectively, for 250 (lower plots) and 9.5 GHz (upper plots). All calculations were made using the 250-GHz magnetic parameters given in Table I and assumed isotropic Brownian rotational diffusion with $\epsilon = 1$. The solid lines show the total width terms obtained by adding these components. The small circles in the results for 250 GHz show the total width terms obtained from a slow-motional analysis.[14]

precisely in the Appendix. Secular, pseudosecular, and nonsecular spectral density functions thus have arguments 0, ω_a, and ω_e, respectively. Contributions to the line width that do not arise from rotation of the magnetic tensors, such as spin-rotational relaxation, broadening due to the presence of molecular oxygen, magnetic field inhomogeneity, and Heisenberg spin exchange are contained in the A' term. The spin transition(s) affected by each J are identified by the frequency argument of the spectral density function and by the subscript, which gives the net change in $(m_S + m_I)$, the z component of the electron spin and nuclear spin, respectively.

The important features of the field and τ_R dependence of the measurable spectral densities appearing in eq 2 are illustrated in Figure 4 for a typical nitroxide probe undergoing isotropic Brownian diffusion. The most apparent influence of magnetic field appears in the A and B terms, namely in the $J_0^{GG}(0)$ secular spectral density, which depends quadratically on the spectrometer field B_0 and contributes to A, and the $J_0^{DG}(0)$ secular spectral density, which is linear in B_0 and contributes to B, which follows from eqs 10–18 in the Appendix. These dependences lead to a large enhancement of both spectral densities at 250 GHz, so that they dominate A_{250} and B_{250}, respectively, and they cause a large separation between A_{250}, B_{250}, and C_{250}. Another significant effect

of the field evident in Figure 4 is that the maxima in the nonsecular spectral densities (i.e., the $J_m^{ij}(\omega_e)$ with i, j = D or G) are shifted at 250 GHz to very small τ_R values (approximately 6.4×10^{-13} s). This greatly suppresses their importance for typical experimental values of $\tau_R > 10^{-12}$ s. (Of course, for $\tau_R < 6.4 \times 10^{-13}$ s (i.e., in the limit of extreme motional narrowing) the $J_m^{GG}(\omega_e)$ and $J_1^{DG}(\omega_e)$ have respective simple quadratic and linear dependences on B_0 as do their secular counterparts.)

One should also note that due to the much larger line widths at 250 GHz for a given τ_R, the limit of motional narrowing corresponds to significantly smaller τ_R values than at 9.5 GHz (i.e., at 9.5 GHz, motional narrowing occurs for $\tau_R < 10^{-9}$ s, whereas for 250 GHz it requires $\tau_R < 10^{-10}$ s). The small circles in Figure 4a–c represent A_{250}, B_{250}, and C_{250} calculated from the predictions of the slow-motional line-shape theory,[14] and illustrate the small deviations from the fast-motion line-width expressions due to incipient slow-motional effects when $1 \times 10^{-10} < \tau_R < 3 \times 10^{-10}$ s. Thus, the onset of slow-motional effects in a given solvent occurs at a higher temperature for 250 GHz.

Another constraint for linearity of A, B, and C with τ_R is, in principle, also required,[1-4] viz., that $\tau_R^2 \ll \omega_a^{-2}$, where ω_a is a measure of the nuclear spin resonance frequency including anisotropic terms (and corresponds to the combination of m and m' in eq 17 in the Appendix that produces the maximum absolute value of ω_a). At 9.5 GHz one obtains $\omega_a^{-1} = 4.7 \times 10^{-9}$ s, whereas at 250 GHz one has 8.5×10^{-10} s. Thus, one finds that this constraint is already satisfied by the slow-motional constraints just noted, such that τ_R is restricted to $<10^{-9}$ s at 9.5 GHz and to $<10^{-10}$ s at 250 GHz.

At 9.5 GHz the $J_0^{GG}(0)$ and $J_0^{DG}(0)$ secular spectral densities are smaller by respective factors of about 690 and 26 compared to their values at 250 GHz. In addition, the maxima of the nonsecular spectral densities for 9.5 GHz also appear at a much longer correlation time, corresponding to $\tau_R = 1.7 \times 10^{-11}$ s, so they can be important for experimentally accessible values of τ_R. As a result, the A term is now dominated by $J_1^{DD}(\omega_a)$, and for $\tau_R < 1.7 \times 10^{-11}$, $J_M^{DD}(\omega_e)$ as well, so that A is of a magnitude similar to C, which depends on $J_0^{DD}(0)$ and $J_1^{DD}(\omega_a)$, with only a weak contribution from $J_1^{DD}(\omega_e)$. In fact, at 9.5 GHz, A, B, and C are all comparable in magnitude.

These features have different consequences for the sensitivities of the line widths measured at high versus low frequency to different types of motional effects. Perhaps the most significant new feature of the linewidths measured at 250 GHz is the tremendous enhancement of the A_{250} parameter. Whereas $A_{9.5}$ is generally not useful for interpreting the rotational dynamics because of contamination from A', at the higher frequency A' is usually negligible with respect to A_{250}, since the types of terms attributed to A' are expected to be largely field-independent.[1,2] Moreover, the A_{250} term reflects the motional modulation of the g tensor, while the line widths measured at low frequency depend mainly on motional modulation of the hyperfine tensor. Since the g tensor has appreciable rhombic character in contrast to the nearly axial symmetry of the hyperfine tensor, the A_{250} parameter should provide more sensitivity to rotational anisotropy and molecular ordering effects.

On the other hand, given that the line widths measured at 250 GHz are relatively insensitive to the nonsecular spectral densities for typical τ_R values, they will not be sensitive to high-frequency dynamical processes such as torques exerted on the spin probe that fluctuate on a time scale comparable with probe reorientation. In contrast, nonsecular terms can be significant at 9.5 GHz, and deviations from the limiting case of Brownian motion are more readily apparent. This type of effect is usually[2,3] accounted for by introducing the empirical parameter ϵ (with $\epsilon > 1$) into the reduced nonsecular spectral densities:

$$j^K(\omega) = \frac{\tau_K}{1 + \epsilon \tau_K^2 \omega^2} \tag{3}$$

which appear in the expressions for the full spectral densities as discussed in the Appendix. In the limiting case of Brownian rotational diffusion, $\epsilon = 1$. The value of ϵ can be relatively accurately determined in many cases,[1-4] although the interpretation of ϵ in terms of a specific physical model may be ambiguous from low-frequency data alone.

In the following we restrict our analysis to include only data for which the contributions of the nonsecular terms to the spectral densities are negligible. This range may be determined by the linearity of the linewidth parameters A, B, and C vs η/T, as well as consistency in the analysis with the values of τ_R (which can be related to the τ_K by eq 18 of the Appendix) that are obtained (note that $\tau_R \propto \eta/T$).

Determination of the Rotational Diffusion Tensor. As we have discussed, once the nonsecular spectral densities may be neglected (because $\omega_e^2 \tau_R^2 \gg 1$), and the secular/pseudosecular reduced spectral densities may be approximated as $j^K(\omega_s) \approx j^K(\omega_a) \approx \tau_K$, then the A, B, and C parameters are all proportional to τ_R, so that the ratios of these parameters are independent of τ_R, and they can be related directly to the anisotropy of the diffusion tensor.[1,15,16]

Only the C/B ratio has been used to measure rotational anisotropy at conventional EPR frequencies, as we have discussed above. The experimental value of C/B imposes a linear constraint on the anisotropy parameters that may be most succinctly expressed in the form of the "allowed-values" equation (AVE) given by Kowert:[15]

$$\alpha_{CB}\rho_x = \beta_{CB}\rho_y + \gamma_{CB} \tag{4}$$

where

$$\alpha_{CB} = A_-\left(\frac{C}{B}G_- - \frac{5}{16}A_-\right)$$

$$\beta_{CB} = A_+\left(-\frac{C}{B}G_+ + \frac{5}{16}A_+\right)$$

$$\gamma_{CB} = 4F_A^{(0)}\left(-\frac{C}{B}F_g^{(0)} + \frac{5}{16}F_A^{(0)}\right) \tag{5}$$

and $G_\pm$ and $A_\pm$ are expressed in terms of the spherical tensor components defined in the Appendix:[17]

$$G_\pm = F_g^{(0)} \bullet \sqrt{6}F_g^{(2)}$$

$$A_\pm = F_A^{(0)} \pm \sqrt{6}F_A^{(2)} \tag{6}$$

In general, the rotational diffusion tensor cannot be fully determined using eqs 4 and 6 at a single frequency without introducing additional assumptions. For example, one usually restricts the diffusion tensor to axial symmetry about the x, y, or z axes by imposing the linear constraints $\rho_x = 1$, $\rho_y = 1$, or $\rho_x = \rho_y$, respectively. The addition of a second linear constraint then permits the rotational anisotropy to be fully determined, subject to the given assumptions.

At frequencies high enough that A' can be neglected, the ratio of A and B should also reflect the rotational anisotropy. An AVE similar to (4) can be written for the A/B ratio at high field. On the basis of the above discussion appropriate for 250 GHz, we neglect $J_1^{DD}(\omega_a)$ with respect to $J_0^{GG}(0)$ in the A term to obtain

$$\alpha_{AB}\rho_x = \beta_{AB}\rho_y + \gamma_{AB} \tag{7}$$

with

$$\alpha_{AB} = G_-\left(\frac{A}{B}A_- - \frac{1}{2}G_-\right)$$

$$\beta_{AB} = G_+\left(-\frac{A}{B}A_+ + \frac{1}{2}G_+\right)$$

$$\gamma_{AB} = 4F_g^{(0)}\left(-\frac{A}{B}F_A^{(0)} + \frac{1}{2}F_g^{(0)}\right) \quad (8)$$

The approximation of neglecting $J_1^{DD}(\omega_a)$ is not strictly necessary, but it does simplify the equation to a form analogous to eq 4, and it does not introduce any significant error as long as eq 7 is applied to A/B ratios obtained at sufficiently high frequency (i.e., 250 GHz).

Equation 7 provides the second linear constraint that can be used in combination with eq 4 to fully determine the rotational diffusion tensor **R**. Ideally one would want to measure both A/B and C/B at 250 GHz to obtain the necessary two constraints. But, as discussed in the previous section, C_{250} could not be measured accurately enough under the present experimental conditions, and it was necessary to employ the C/B ratio determined at lower field.

Equation 7 is of significant utility only at fields high enough that A is dominated by the J^{GG} spectral densities. At lower fields, where A and C both reflect primarily the J^{DD} spectral densities (cf. Figures 4A and 4C), the A/B ratio provides little additional information beyond that already available in C/B. However, because of the different symmetries of the g and hyperfine tensors, the AVE for A/B at 250 GHz provides a linear constraint on ρ_x and ρ_y that is essentially independent of the AVE for C/B. (Note that this last statement is true whether C/B is obtained at high or lower frequency). Thus, high field is necessary to provide a sufficient degree of independence between the two linear equations for ρ_x and ρ_y that the rotational diffusion tensor may fully determined without any simplifying assumptions aside from that of Brownian motion.

We demonstrate this method for pd-Tempone diffusing in toluene-d_8 using the experimental A_{250}/B_{250} ratio, and the $C_{9.5}/B_{9.5}$ ratio that has previously been obtained for this system.[2] Figure 5 shows a plot of the two AVEs for toluene solvent, using the magnetic parameters obtained at 250 GHz that are given in Table I. The intersection of the two lines occurs at $\rho_x = 1.8 \pm 0.2$, $\rho_y = 1.5 \pm 0.3$ (more precisely $\rho_x = 1.78 \pm 0.24$, $\rho_y = 1.47 \pm 0.29$). The error estimates for ρ_x and ρ_y were based on the measured uncertainties in A_{250}/B_{250}, $C_{9.5}/B_{9.5}$ and in the magnetic parameters, and were determined from an error analysis based on eqs 4–8 following standard procedures.[18] The error analysis also indicated some positive correlation in the uncertainties of ρ_x and ρ_y such that $\rho_x = (1.2 \pm 0.1)\rho_y$. (We show in Figure 5 the error ellipse for (ρ_x, ρ_y) derived from our analysis). Thus, the two AVEs indicate a modest preference for the x molecular axis (along the N–O bond of PDT) as the axis of fastest rotation, with the z molecular axis (parallel to the p–π orbital centered on the N atom) the axis of slowest rotation. This is a small but significant correction to the earlier conclusion of isotropic rotation ($\rho_x = \rho_y = 1$) based on just the 9.5 GHz data of Hwang et al.[2] and the assumption of axial symmetry.

We have also analyzed the sensitivity of the uncertainties in ρ_x and ρ_y to the accuracy of the measured parameters following standard procedures.[18] We found that because of the high accuracy to which the principal components of the g tensor (especially their relative values, accurate to 0.2%) could be obtained, their uncertainty made a negligible contribution to the final result. The overall error was due to the contributions of all the other parameters, although the error in A_{250}/B_{250} made a significantly larger overall contribution than that in $C_{9.5}/B_{9.5}$ and in the hyperfine tensor. (The error in $C_{9.5}/B_{9.5}$ contributed only negligibly to the uncertainty in ρ_x but was significant for ρ_y.) Note that both linewidth parameter ratios were determined to 2% accuracy and the most important hyperfine tensor component

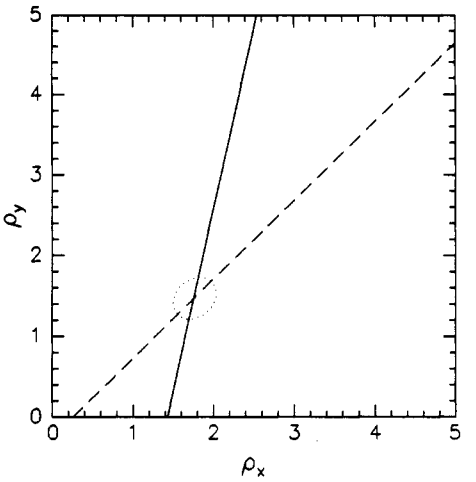

Figure 5. Determination of anisotropy parameters ρ_x and ρ_y for PDT in toluene-d_8 using two allowed-value equations as described in the text. Solid and dashed lines show the AVE's for the A_{250}/B_{250} and the C_{250}/B_{250} ratios, respectively, which intersect at $\rho_x = 1.8$ and $\rho_y = 1.5$. The ellipse plotted about this intersection indicates the uncertainty in this intersection point as determined by the error analysis (cf. text).

(which is $F_A^{(0)}$, since $F_A^{(2)}$ is very small) is accurate to 1%. Had we used the g tensor components measured at 9.5 GHz with their 6% uncertainties, they would have been the predominant sources of error in ρ_x and ρ_y, and this would have doubled the total uncertainties in those anisotropy parameters. We may conclude that improvements in the accuracy of ρ_x and ρ_y would be achieved mainly by more accurate measurements of the linewidth parameter ratios but also of the hyperfine tensor. One may hope to improve the signal-to-noise at 250 GHz by potential instrumental improvements already described,[9] and this should make it possible to improve upon the accuracy of measuring A_{250}/B_{250}, as well as the components of the A-tensor from rigid limit simulations. Of course, substantial signal averaging with existing equipment would be expected to help. Improvements in obtaining $C_{9.5}/B_{9.5}$ accurately might be achieved by performing T_2 measurements by electron-spin-echoes (ESE), thereby avoiding the need to correct for inhomogeneous broadening from the unresolved deuterons.[19] ESE performed in a two-dimensional Fourier transform format[19] would have the added advantage of yielding all three hyperfine T_2^{-1}'s simultaneously, permitting a more reliable determination of their differences.

Our analysis has shown that the somewhat different prediction of Hwang et al.[2] was a result of (a) the use of only the $C_{9.5}/B_{9.5}$ ratio, (b) the use of less accurate magnetic tensors measured at 9.5 GHz, and (c) a small numerical inaccuracy in their analysis.

Once ρ_x and ρ_y are obtained, then the optimum value of τ_R (as a function of T or η/T) may be determined. Following Zager and Freed,[3] we let

$$\tau_R = \frac{4\pi r_e^3 \eta}{3k_B T} + \tau_R^0 \quad (9)$$

which implies (modified) Stokes–Einstein-type behavior where r_e is an average hydrodynamic radius (cf. Appendix) and τ_R^0 is an empirical intercept. The set of data (A_{250}, B_{250}, $B_{9.5}$, $C_{9.5}$) over the η/T range used above for determining ρ_x and ρ_y was then utilized to obtain the best estimate for τ_R. The solid lines in Figure 2 show the line-width predictions obtained from the theoretical equations with the experimentally determined $(\rho_x,\rho_y) = (1.8,1.5)$, $r_e = 2.15 \pm 0.05$ Å, and $\tau_R^0 = (2 \pm 2) \times 10^{-12}$ s. (Note that in ref 3 an $r_e = 2.0$ Å was obtained based on the original low-frequency study of Hwang et al.[2])

Now, by extrapolating this analysis into the extreme narrowing regime for 9.5 GHz and allowing ϵ (cf. eq 3) to vary in order to fit the $C_{9.5}$ and $B_{9.5}$ data in this regime, we may obtain a new and presumably more reliable estimate of this parameter. (That is,

we are now relaxing our restriction of using only data for which nonsecular terms make negligible contributions; cf. above.) We found $\epsilon = 4.5 \pm 1.5$ vs the previous estimate[2] of 5.4, and this value is used in the solid curves shown in Figure 2. We also display in Figure 2, for comparison, the fit to an isotropic diffusion model for which $\rho_x = \rho_y = 1$ by the dashed lines. While B_{250} and $B_{9.5}$ are well fit, this is less so for A_{250} and $C_{9.5}$. The discrepancy is most evident in the A_{250}/B_{250} and $C_{9.5}/B_{9.5}$ ratios predicted by the isotropic model, which are respectively 5.1 and 0.985 compared with the experimental values of 5.5 ± 0.1 and 0.925 ± 0.016. At this point it is important to emphasize that the distinction between an isotropic model and the modest anisotropy we obtain is based on the accuracy with which the ratios A_{250}/B_{250} and $C_{9.5}/B_{9.5}$ are determined from plots like that of Figure 3. This involves the simultaneous use of all the data in Figure 2. There is clearly some scatter in the data of Figure 2, but the predicted (and observed) constancy of the ratio of A_{250}/B_{250} (and/or $C_{9.5}/B_{9.5}$) over the relevant range of η/T studied permits us to utilize all our experimental points to obtain a much more accurate *average* A_{250}/B_{250} and $C_{9.5}/B_{9.5}$ than would appear from the scatter of individual points in Figure 2 (or 3).

We now compare the experimental values for ρ_x and ρ_y with the predictions of a Perrin–Stokes–Einstein (PSE) model described previously,[2,16] utilizing the radii a_i around each of the molecular axes, which are[20] $a_x = 4.2$ Å, $a_y = 2.7$ Å, and $a_z = 3.0$ Å. We obtain from this model $\rho_x = 1.35 \pm 0.07$ and $\rho_y = 0.97 \pm 0.05$ (utilizing the uncertainties reported in ref 20). It is also possible to define an average hydrodynamic radius, r_e, for this model as outlined in the Appendix. We obtain $r_e = 3.2$ Å, which is the same as that obtained previously[2] assuming axial symmetry.

The difference between the r_e measured from the experiment and that based upon molecular dimensions is typical and is usually explained either by introducing slip[2,3] in the rotational diffusion or by using an "expanded volume" model.[3] The hydrodynamic PSE model does predict a preference for rotation about the molecular x axis, consistent with our results, although we find a somewhat larger ρ_x. Also, we find $R_x/R_y = 1.2 \pm 0.1$ vs the value of 1.39 predicted by the PSE model. Given our uncertainties, the comparison is not at all unreasonable. However, we do not wish to suggest the general applicability of the hydrodynamic PSE model for anisotropic rotational diffusion. One should perform more studies with a range of uncharged nitroxides of different shapes in a range of non hydrogen-bonding solvents to test the anisotropic aspects of the PSE model vs specific intermolecular interactions. Other questions, such as any deviations of the observed rotational correlation time from the linear relationship $\tau_R \propto \eta/T$, as well as the magnitude of the associated proportionality constant, have been discussed previously.[1-4]

Other than rotational anisotropy, there are two other physical effects that can in principle also influence the apparent A/B and C/B ratios of the diffusing spin probe, which we will discuss briefly. These include (i) a rotation of the A- and/or g-tensor principal axes away from those of the rotational diffusion tensor and (ii) internal motion of the spin probe such as the alternation of pd-Tempone between different twisted-boat configurations.

A misalignment of the principal axes of either the A or g tensor with respect to the principal axes of $\mathbf{R}$ would alter B and at least one other linewidth parameter in comparison with the case where the g- and A-tensor axes coincide. The physical effect of introducing such a misalignment is to change the specific way in which the components of the misaligned tensor are averaged by the rotational motion. For PDT, only misalignment of the z axes of the two tensors would produce any appreciable effect, since the x and y principal values of the A tensor are so similar in this species. However, there is no evidence for this type of effect in the extensive body of spectroscopy on this common nitroxide probe, including a single-crystal EPR and ENDOR study.[21]

The effects of internal motions on the motionally narrowed linewidths of pd-Tempone have been considered previously.[2] An internal motion that shifts the orientations of the g- and A-tensor axes would affect all three line-width parameters to some extent. Since internal dynamic processes should also obey very different temperature and viscosity dependences from those of overall molecular rotation, one would expect some deviations from linear dependence on η/T for the line-width parameters. Also, if the g and A tensors were somewhat differently affected by the internal motion, the effect should be somewhat different for each of the three line-width parameters.

At 9.5 GHz, the $B_{9.5}$ and $C_{9.5}$ parameters have the same slope on a log–log plot vs η/T over the range of τ_R values where nonsecular contributions are unimportant. This result was used to suggest that internal motion is at most only a minor contribution to the spin relaxation.[2] Studies as a function of pressure[3] on this same system support this. If A (or B) is particularly sensitive to internal motions this should be evident in the line-width parameters measured at high frequency. However, even at 250 GHz, there is no evidence that A_{250} and B_{250} exhibit any significant nonlinearity with respect to η/T (cf. Figure 2), providing a further indication that internal motions are relatively unimportant for electron spin relaxation in PDT.

Conclusions

Motionally narrowed spectra obtained at an EPR frequency of 250 GHz have been presented for the PDT nitroxide spin label in toluene-d_8. These results demonstrate that, in contrast to motional-narrowing studies at conventional EPR frequencies, the A line-width parameter measured at 250 GHz is useful in the analysis of the rotational dynamics of the spin probe.

The ratio of the A_{250} and B_{250} line-width parameters can be used to place an "allowed-value" constraint on the anisotropy parameters of the diffusion tensor, $\rho_x = R_x/R_z$ and $\rho_y = R_y/R_z$, in addition to the constraint imposed by the C/B ratio, which may in principle also be measured at high frequency, but is at present more accurately measured at conventional EPR frequencies for $\omega_e^2\tau_R^2 \gg 1$. The A_{250} line-width parameter is determined by the g tensor, whereas C at any frequency is determined by the hyperfine tensor. Thus, the constraints imposed by the experimental A_{250}/B_{250} and $C_{9.5}/B_{9.5}$ ratios are independent, and can be used to determine all components of the rotational diffusion tensor. The fact that $B_{250}/B_{9.5}$ is found to equal the ratio of the two frequencies, in exact agreement with theory, is taken as excellent confirmation of the validity of motional narrowing methods for studying rotational dynamics in EPR, and it provides a consistency check on the data obtained at the two frequencies. Utilizing motional narrowing results from PDT in toluene-d_8 at 250 and 9.5 GHz, our analysis yields $\rho_x = 1.8 \pm 0.2$ and $\rho_y = 1.5 \pm 0.3$. These results show similar trends to those of the hydrodynamic Perrin–Stokes–Einstein model. The good precision in such studies is significantly aided by the improved accuracy with which the g tensor can be measured from rigid limit spectra obtained at 250 GHz. These results for a case exhibiting only small deviations from anisotropy illustrate the degree of accuracy available by current methods in measuring the components of $\mathbf{R}$. Once the anisotropy parameters of $\mathbf{R}$ are reliably determined, the extreme motional narrowing regime (i.e., $\omega_e^2\tau_R^2 \ll 1$) at the lower frequency may be analyzed for non-Brownian deviations, as also illustrated in this work.

Acknowledgment. We are grateful to Mr. Franck Arntzen for his assistance with the X-band spectroscopy of our samples and Dr. W. Bryan Lynch for his expert assistance with the 250 GHz EPR instrumentation.

Appendix: Expressions for Fast-Motional Nitroxide Line Widths at High Field

To obtain explicit expressions for the J functions given in eq 2 in terms of the magnetic tensors and dynamic parameters we start from the formulae derived by Hwang et al.[2] from a

perturbation analysis of the full stochastic Liouville equation. Their expressions neglect the ^{14}N nuclear Zeeman energy, which is typically omitted in nitroxide work because it is assumed to be much smaller than the *END* interaction. However, at 250 GHz the ^{14}N nuclear Zeeman and *END* energies are quite comparable, and it becomes necessary to include them both into the expressions for the spin transition frequencies. A second limitation of the equations given by Hwang et al. is the assumption of an axial diffusion tensor. We present here a modified treatment appropriate for motionally narrowed nitroxide line widths at EPR frequencies above approximately 50 GHz.

The spectral densities given in eq 2 may be written explicitly as

$$J_0^{GG}(0) = {}^1/_{20}\sum_{K=-2}^{2}(\mathcal{F}_g^{(K)})^2 j^K(\omega_{s,0}^K)$$

$$J_1^{GG}(\omega_e) = {}^1/_{20}\sum_{K=-2}^{2}(\mathcal{F}_g^{(K)})^2 j^K(\omega_e) \qquad (10)$$

for the GG terms

$$J_0^{DG}(0) = {}^1/_{20}\sum_{K=-2}^{2}(\mathcal{F}_A^{(K)}\mathcal{F}_g^{(K)})\sum_{m'=-1,1} j^K(\omega_{s,m'}^K)$$

$$J_1^{DG}(\omega_e) = {}^1/_{20}\sum_{K=-2}^{2}(\mathcal{F}_A^{(K)}\mathcal{F}_g^{(K)}) j^K(\omega_e) \qquad (11)$$

for the DG terms, and

$$J_0^{DD}(0) = {}^1/_{20}\sum_{K=-2}^{2}(\mathcal{F}_A^{(K)})^2\sum_{m'=-1,1} j^K(\omega_{s,m'}^K)$$

$$J_1^{DD}(\omega_a) = {}^1/_{20}\sum_{K=-2}^{2}(\mathcal{F}_A^{(K)})^2\sum_{m,m'=-1,1} j^K(\omega_{a,m,m'}^K)$$

$$J_0^{DD}(\omega_e) = {}^1/_{20}\sum_{K=-2}^{2}(\mathcal{F}_A^{(K)})^2 j^K(\omega_e)$$

$$J_1^{DD}(\omega_e) = J_2^{DD}(\omega_e) = J_0^{DD}(\omega_e) \qquad (12)$$

for the DD terms. The $\mathcal{F}_A$'s and $\mathcal{F}_g$'s appearing in eqs 12–16 are the spherical components of the A and g tensors transformed into the "normal-mode" basis in which the asymmetric diffusion operator is diagonal.[16] These may be obtained from the spherical components of the magnetic tensors expressed in the principal axis system of the diffusion tensor, $F_\mu^{(K)}$ ($\mu = g,A$) according to the standard transformation given by Freed.[16] If the rotational diffusion tensor is coaxial with the g and A tensors, the only nonzero terms in the summations appearing in eqs 10–12 are for $K = 0$ and $K = 2$, and the transformation can be written

$$\mathcal{F}_\mu^{(0)} = \frac{a}{N_-}F_\mu^{(0)} + \frac{b_-}{N_-}F_\mu^{(2)}\sqrt{2}$$
$$\mathcal{F}_\mu^{(2)} = \frac{a}{N_-}F_\mu^{(0)} + \frac{b_+}{N_+}F_\mu^{(2)}\sqrt{2} \qquad (13)$$
$$\mathcal{F}_\mu^{(-2)} = 0$$

where the coefficients a, $b_\pm$, and $N_\pm$ depend upon the anisotropy parameters of the diffusion tensor $\rho_x = R_x/R_z$ and $\rho_y = R_y/R_z$:[22]

$$a \equiv 12^{1/2}R^{(2)};\quad b_\pm \equiv 2(R^{(0)} \pm \Delta);\quad N_\pm \equiv 2[2\Delta(\Delta \pm R^{(0)})]^{1/2}$$

$$\Delta \equiv [3(R^{(2)})^2 + (R^{(0)})^2]^{1/2};\quad R^{(0)} \equiv R_z\left(1 - \frac{1}{2}(\rho_x + \rho_y)\right);$$
$$R^{(2)} \equiv (R_z/2)(\rho_x - \rho_y) \qquad (14)$$

and the F_μ's are the spherical components of the magnetic tensors expressed in the common molecular frame:

$$F_A^{(0)} = ({}^2/_3)^{1/2}(A_{zz} - {}^1/_2(A_{xx} + A_{yy}));\quad F_A^{(2)} = {}^1/_2(A_{xx} - A_{yy})$$

$$F_g^{(0)} = ({}^2/_3)^{1/2}(g_{zz} - {}^1/_2(g_{xx} + g_{yy}))\beta_e B_0/\hbar;$$
$$F_g^{(2)} = {}^1/_2(g_{xx} - g_{yy})\beta_e B_0/\hbar \qquad (15)$$

The j^K reduced spectral density functions in eqs 10–12 are defined using the eigenvalues of the diffusion operator in the normal-mode basis. As a result of eq 13, only the following are needed:

$$j^K(\omega) = \frac{\tau_K}{1 + \epsilon(\tau_K)^2\omega^2}$$

$$(\tau_0)^{-1} = 2[(R_x + R_y + R_z) - \Delta]$$

$$(\tau_2)^{-1} = 2[(R_x + R_y + R_z) + \Delta] \qquad (16)$$

where $\epsilon = 1$ for simple Brownian motion. The secular and pseudosecular transition frequencies ω_s^K and ω_a^K appearing in eqs 10–12 are given by

$$\omega_{s,m'}^K = (-1)^{K/2}\frac{2\sqrt{6}}{21}[F_g^{(0)} + m'F_A^{(0)}] \quad (m, m' = \pm 1)$$

$$\omega_{a,m,m'}^K = \omega_n + m\frac{\bar{a}}{2} + (-1)^{K/2}\frac{\sqrt{6}}{21}[F_g^{(0)} + m'F_A^{(0)}]$$
$$(m, m' = \pm 1)$$

$$\bar{a} = -{}^1/_3(A_x + A_y + A_z) \qquad (17)$$

Finally, the rotational correlation time of the probe τ_R is defined as

$$\tau_R = \tau_0\left(\frac{2\tau_2}{3\tau_0 - \tau_2}\right)^{1/2} \qquad (18)$$

This convention for τ_R was chosen so that, in the limiting case of axially symmetric rotation, (i.e., for $R_\perp = R_x = R_y$ and $R_\parallel = R_z$), Equation 18 reduces to the definition $\tau_R^{-1} = 6(R_\perp R_\parallel)^{1/2}$ given previously for axial diffusion.[2]

Second-Order Perturbation Corrections. In the incipient slow-motional region, the secular and pseudosecular transition frequencies undergo small shifts, which appear in square brackets in eq 17. These terms produce second-order contributions to the B parameter (denoted by single primes):

$$J_0^{GG'}(0) = \sum_{K=0,2}(\mathcal{F}_g^{(K)})^2({}^1/_2)[j^K(\omega_{s,1}^K) - j^K(\omega_{s,-1}^K)]$$

$$J_0^{DD'}(0) = \sum_{K=0,2}(\mathcal{F}_A^{(K)})^2({}^1/_2)[j^K(\omega_{s,1}^K) - j^K(\omega_{s,-1}^K)]$$

$$J_1^{DD'}(\omega_a) = \sum_{K=0,2}(\mathcal{F}_A^{(K)})^2({}^1/_2)\sum_{m=-1,1}[j^K(\omega_{a,m,1}^K) - j^K(\omega_{a,m,-1}^K)] \qquad (19)$$

and also a second-order contribution to the C parameter (denoted

by a double prime):

$$J_0^{GG''}(0) = \sum_{K=0,2} (\mathcal{F}_g^{(K)})^2[{}^1/_2(j^K(\omega_{s,1}^K) + j^K(\omega_{s,-1}^K)) - j^K(\omega_{s,0}^K)] \quad (20)$$

At the 250 GHz, the terms given in eqs 19 and 20 become significant for $\tau_R > 10^{-10}$ s.

Determining Effective Radius of Rotation for Fully Anisotropic Diffusion. The components of the diffusion tensor **R** are related to the friction tensor β of the diffusing particle by[16]

$$R_i = k_B T/\beta_i \quad (21)$$

Within the context of the Perrin–Stokes–Einstein model, one may compute the components of the friction tensor if the lengths of the principal axes of the diffusing ellipsoid are known. One finds that the components of β are proportional to a quantity γ that depends only upon the geometry of the ellipsoid. For the ith axis

$$\gamma_i = \frac{a_j^2 + a_k^2}{a_j^2 Q_j + a_k^2 Q_k} \qquad i \neq j \neq k \quad (22)$$

where the a_i are the lengths of the principal axes of the ellipsoid, and the Q_i are the elliptic integrals:

$$Q_i = \int_0^\infty ds/[(a_i^2 + s)^3(a_j^2 + s)(a_k^2 + s)]^{1/2} \quad (23)$$

The anisotropy parameters ρ_x and ρ_y are simply related to the γ_i: $\rho_x = \gamma_z/\gamma_x$ and $\rho_y = \gamma_z/\gamma_y$. By equating the Stokes–Einstein equation (eq 9, with $\tau_R^0 = 0$) with the definition of τ_R given in eq 18 above, one may compute the effective radius of the ellipsoid in the Perrin–Stokes–Einstein model:

$$r_e^3 = 2\gamma_z/[(\rho_x - \delta)(\rho_s + 2\delta)]^{1/2} \quad (24)$$

where $\rho_s = \rho_x + \rho_y + 1$ and $\delta = \Delta/R_z$. This expression yields $r_e = a$ in the isotropic limit of $a_i = a$ for $i = x, y, z$.

References and Notes

(1) (a) Goldman, S. A.; Bruno, G. V.; Polnaszek, C. F.; Freed, J. H. *J. Chem. Phys.* **1972**, *56*, 716. (b) Goldman, S. A.; Bruno, G. V.; Freed, J. H. *Ibid.* **1973**, *59*, 3071.

(2) Hwang, J. S.; Mason, R. P.; Hwang, L.-P.; Freed, J. H. *J. Phys. Chem.* **1975**, *79*, 489.

(3) Zager, S. A.; Freed, J. H. *J. Chem. Phys.* **1982**, *77*, 3344, 3360.

(4) Polnaszek, C. F.; Freed, J. H. *J. Phys. Chem.* **1975**, *79*, 2283.

(5) Meirovitch, E.; Igner, D.; Igner, E.; Moro, G.; Freed, J. H. *J. Chem. Phys.* **1982**, *77*, 3915.

(6) Tanaka, H.; Freed, J. H. *J. Phys. Chem.* **1985**, *89*, 350.

(7) Hwang, J. S.; Rao, K. V. S.; Freed, J. H. *J. Phys. Chem.* **1976**, *80*, 1490.

(8) Lynch, W. B.; Earle, K. A.; Freed, J. H. *Rev. Sci. Instrum.* **1988**, *59*, 1345.

(9) Budil, D. E.; Earle, K. A.; Lynch, W. B.; Freed, J. H. *Advanced EPR: Applications in Biology and Biochemistry*, Hoff, A. J., Ed.; Elsevier: Amsterdam, 1989; Chapter 8.

(10) Ondar, M. A.; Grinberg, O. Ya.; Dubinskii, A. B.; Shestakov, A. F.; Lebedev, Ya. S. *Khim. Fiz.* **1983**, *2*, 54.

(11) More, J. J.; Garbow, B. S.; Hillstrom, K. E. *Users' Guide for MINPACK-1*; publication ANL 80-74; National Technical Information Service: Springfield, VA, 1980.

(12) Nayeem, A.; Rananavare, S. B.; Sastry, V. S. S.; Freed, J. H. *J. Chem. Phys.* **1989**, *91*, 6887.

(13) Barlow, A. J.; Lamb, J.; Matheson, A. J. *Proc. R. Soc. London Ser. A* **1966**, *292*, 322.

(14) Schneider, D. J.; Freed, J. H. *Biological Magnetic Resonance*, Vol. 8, Berliner, L. J., Reuben, J., Eds.; Plenum: New York, 1989; p 1.

(15) Kowert, B. A. *J. Phys. Chem.* **1981**, *85*, 229.

(16) Freed, J. H. *J. Chem. Phys.* **1964**, *41*, 2077.

(17) The spherical tensor components Δa, δa, Δg, and δg used by Kowert[15] are related to those given in the Appendix by $\Delta a = (3/2)^{1/2}F_A^{(0)}$, $\delta a = F_A^{(2)}$, and similarly for the g-tensor components. The equivalence of eq 4 to Kowert's AVE can be seen by substituting these expressions into the equation and multiplying by $^2/_3$.

(18) Bevington, P. R. *Data Reduction and Error Analysis for the Physical Sciences*; McGraw-Hill, New York, 1969; Chapter 4.

(19) Gorcester, J.; Millhauser, G. L.; Freed, J. H. *Advanced EPR: Applications in Biology and Biochemistry*; Hoff, A. J., Ed. Elsevier: Amsterdam, 1989; Chapter 5.

(20) Shibaeva, R. P.; Atovmyan, L. O.; Neiganz, M. G.; Novakovskaya, L. A.; Ginzburg, S. L. *Zh. Strukt. Khim.* **1972**, *13*, 42.

(21) Brustolon, M.; Maniero, A. L.; Corvaja, C. *Mol. Phys.* **1984**, *51*, 1269.

(22) As has been noted by Freed,[16] the sign of Δ in eq 14 must be chosen so that $\mathcal{F}_\mu^{(K)} \rightarrow F_\mu^{(K)}$ in the limiting case of an axially symmetric diffusion tensor. The proper choice of sign depends upon which molecular axis corresponds to the unique rotational axis in this limit. When the z axis is "most nearly unique", or more rigorously, when $|(1 - \rho_x)(1 - \rho_y)| > (\rho_x - \rho_y)^2$, Δ should be chosen to have the same sign as $R^{(0)}$; otherwise, Δ and $R^{(0)}$ should have opposite signs.